Active Absorption of Irregular Gravity Waves in BEM-Models

Brorsen, Michael; Frigaard, Peter

Published in:
Boundary Elements XIV

Publication date:
1992

Document Version
Early version, also known as pre-print

Active absorption of irregular gravity waves in BEM-models

M. Brorsen and P. Frigaard
Department of Civil Engineering, Aalborg University, Denmark

ABSTRACT

The boundary element method is applied to the computation of irregular gravity waves. The boundary conditions at the open boundaries are obtained by a digital filtering technique, where surface elevations in front of the open boundary are filtered numerically yielding the velocity to be prescribed at the boundary. By numerical examples it is shown that well designed filters can reduce the wave reflection to a few per cent over a frequency range corresponding to a Jonswap spectrum.

INTRODUCTION

One of the major difficulties with the calculations of water waves is the formulation of open-boundary conditions. In earlier computations with BEM-models, the boundary conditions have been either periodic in space, Longuet-Higgins and Cokelet [9] and Dold and Peregrine [4], or the Sommerfeld radiation has been used, see e.g. Lennon et al. [8] and Brorsen and Larsen [3].

The Sommerfeld radiation condition allows waves of permanent form to leave the domain without any reflection, if the phase velocity of the waves in the model is coinciding with the phase velocity used in the radiation condition. If not so, partial reflection takes place and the reflection increases with increasing difference between the actual phase velocity and phase velocity used in the radiation condition. The Sommerfeld radiation condition can be used in case of irregular linear shallow water waves, because all waves propagate with the same phase velocity, but in general this boundary condition is inadequate even if the phase velocity in the boundary condition corresponds to the peak period of the surface elevation spectrum.

In the paper of Larsen and Dancy [7] another approach to the treatment of open boundaries was put forward. The incident waves are generated inside the boundary and all outgoing waves (internally generated as well as scattered) are absorbed on the open boundaries by use of sponge layers. In that paper a finite-difference model based on the Boussinesq equations was used.

Internally generated waves were used in BEM-modelling by Brorsen and Larsen [3] but the absorption of outgoing waves at the open boundary was, however, achieved by use of a Sommerfeld radiation condition. The sponge layer technique was dropped because the work done by Baker et al. [1] and own preliminary tests too showed that the width of the sponge layer should be at least one wavelength in order to obtain a satisfactory low reflection coefficient. Linear irregular waves can, however, be regarded as the sum of regular waves with different frequency and wavelength, and consequently the width of the sponge layer must be comparable to the largest wavelength of the regular waves. This demands a computational domain so large that it cannot be used in practice due to the necessary amount of computational effort.

It is shown in this paper that these problems can be reduced considerably by a new approach, where the boundary condition at an open boundary is provided by a filtering technique. The surface elevation in front of the boundary is filtered numerically to yield the velocity component with respect to the normal to the boundary. The approach with a boundary condition based on measurements in the domain is in this paper denoted *active* absorption.

MATHEMATICAL FORMULATION

Governing equations

We consider an inviscid irrotational 2-D flow described by a velocity potential φ, and the velocity field is given by

$$\vec{v} = \nabla\varphi = (u, w) \tag{1}$$

where $\nabla = (\partial\ /\partial x\ ,\ \partial\ /\partial z)$ is the 2-D gradient operator.
If we also assume incompressible fluid, the continuity equation becomes a Laplace equation for φ,

$$\nabla^2\varphi = 0 \qquad \text{in } A \tag{2}$$

The sea bed, S_B, is assumed horizontal and impervious, and the waves are in this paper generated by a piston wavemaker.

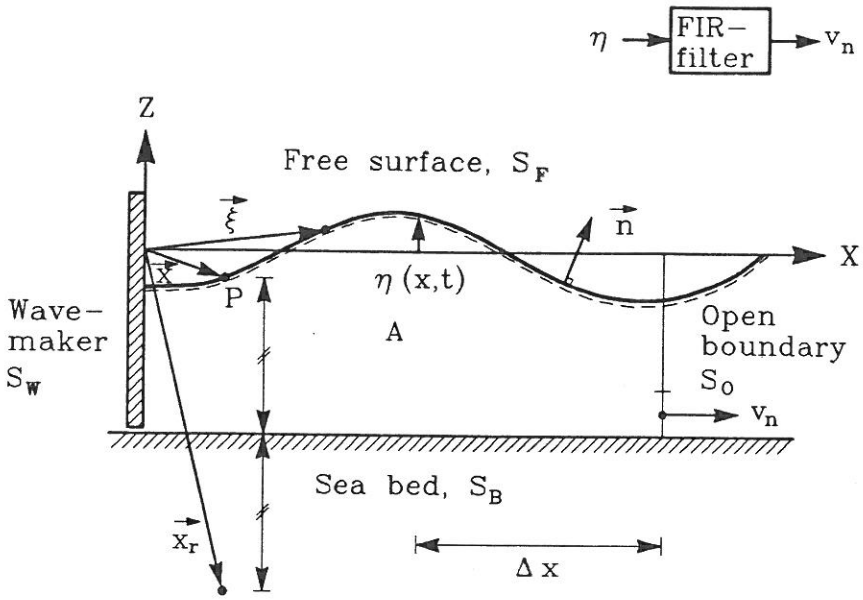

Figure 1. Sketch of the region used in the numerical model. Definition of parameters.

On the open boundary, S_O, the waves shall be allowed to pass without being reflected.

By use of Green's 2. identity the boundary value problem is transformed to a boundary integral equation, and the potential at point P positioned at point $\vec{x}$ is given by

$$\alpha(\vec{x}) \cdot \varphi(\vec{x}) = \int_S \left(\varphi\left(\vec{\xi}\right) \frac{\partial G\left(\vec{x},\vec{\xi}\right)}{\partial n} - G\left(\vec{x},\vec{\xi}\right) \frac{\partial \varphi\left(\vec{\xi}\right)}{\partial n} \right) dA \qquad (3)$$

where S is the boundary of the computational domain A, $\vec{\xi}$ is the position vector of a point on the boundary, $G\left(\vec{x},\vec{\xi}\right)$ is a Green's function and $\alpha(\vec{x})$ is a coefficient depending on the position of P and the geometry of the boundary. The unit outward normal vector is denoted $\vec{n}$, see Figure 1.
In case of constant water depth we use in 2-D models

$$G\left(\vec{x},\vec{\xi}\right) = \ln|\vec{\xi} - \vec{x}| + \ln|\vec{\xi} - \vec{x}_r|$$

where $\alpha = \pi$ if $\vec{x}$ is situated on the boundary, and $\vec{x}_r$ is the position vector of the point which is the reflection of point P into the sea bed. See Fig. 1. Given the necessary boundary conditions, solving of equation (3) gives the variation along the boundary of φ and $\partial\varphi/\partial n$. The applied time stepping method is close to the method described in Dold and Peregrine [4], but the boundary of the computational domain is not moved. This time stepping method requires, however, knowledge of both $\varphi_t = \partial\varphi/\partial t$ and $\partial\varphi_t/\partial n$ on the boundary.

Differentiation of equation (2) with respect to time, gives the Laplace equation for φ_t,

$$\nabla^2 \varphi_t = 0 \tag{4}$$

which is transformed to the corresponding boundary integral equation for φ_t:

$$\alpha\left(\vec{x}\right) \cdot \varphi_t\left(\vec{x}\right) = \int_S \left(\varphi_t\left(\vec{\xi}\right) \frac{\partial G\left(\vec{x},\vec{\xi}\right)}{\partial n} - G\left(\vec{x},\vec{\xi}\right) \frac{\partial \varphi_t\left(\vec{\xi}\right)}{\partial n} \right) dA \tag{5}$$

Solving of equation (5) yields the variation of φ_t and $\partial\varphi_t/\partial n$ along the boundary.

General boundary conditions for φ and φ_t, linear waves

Since we only consider linear waves, the position of the boundary of the computational domain is not changed.
On the free surface, S_F, φ satisfies the linearized kinematic and dynamic boundary conditions, respectively,

$$\frac{\partial \eta}{\partial t} = \frac{\partial \varphi}{\partial n} \qquad \text{on } S_F \tag{6}$$

and

$$\varphi_t = -g\,\eta \qquad \text{on } S_F \tag{7}$$

where g is the acceleration due to gravity.
On the stationary sea bed, S_B, φ and φ_t satisfies

$$\frac{\partial \varphi}{\partial n} = 0 \qquad \text{on } S_B \tag{8}$$

and

$$\frac{\partial \varphi_t}{\partial n} = 0 \qquad \text{on } S_B \tag{9}$$

At the wavemaker the boundary conditions in case of linear waves read

$$\frac{\partial \varphi}{\partial n} = -\dot{x}_w(t) \qquad \text{on } S_O \tag{10}$$

and

$$\frac{\partial \varphi_t}{\partial n} = -\ddot{x}_w(t) \qquad \text{on } S_O \tag{11}$$

where x_w is the position of the wavemaker.

Active absorption, boundary conditions

On the open boundary, S_O, the boundary conditions read

$$\frac{\partial \varphi}{\partial n} = v_n \qquad \text{on } S_O \tag{12}$$

and

$$\frac{\partial \varphi_t}{\partial n} = \frac{\partial v_n}{\partial t} \qquad \text{on } S_O \tag{13}$$

where the velocity component after the normal, v_n, is obtained by numerical filtering of a time series of surface elevation observed the distance Δx in front of the open boundary, see Fig. 1. If the N coefficients of the numerical filter are denoted h^j, $j = -(N-1)/2, \ \ldots \ , (N-1)/2$ and N is an odd integer, v_n^{k+1} is calculated by

$$v_n^{k+1} = \sum_{j=-M}^{j=M} h^j \cdot \eta^{k+1-M+j} \tag{14}$$

where $M = (N-1)/2$ and superscripts denote the no. of time step and filter coefficient, respectively. Thus the velocity can be interpreted as a special mean value of the preceeding N values of the surface elevation.

As stated in e.g. Karl [6], h^j is the impulse response of the filter. If the input to the filter is a unit impulse, i.e. only one η-value (of magnitude 1) is different from zero, the output from the filter is, according to equation (14), equal to the filter coefficients. This type of filter is normally called a FIR-filter, due to the *F*inite duration of the *I*mpulse *R*esponse of the filter.

According to the theory of 1. order Stokes waves (linear waves) the relation between surface elevation and horizontal particle velocity measured in the same vertical is

$$u = 2\pi f \frac{\cosh k(z+h)}{\sinh kh} \eta \tag{15}$$

where $k = 2\pi/L$ is the wave number, L is the wavelength, $f = 2\pi/T$, is the frequency, T is the wave period, and h is the water depth. See e.g. Svendsen and Jonsson [10]. From equation (15) the magnitude of the frequency response of the filter, $|H(f)|$, is seen to be

$$|H(f)| = 2\pi f \frac{\cosh k(z+h)}{\sinh kh} \tag{16}$$

and the phase shift, $\theta(f)$, is zero at all frequencies. Note, however, that $\theta(f) \neq 0$, if η and u are separated the horizontal distance Δx.

The complex frequency response, $H(f)$, can be calculated by

$$H(f) = |H(f)|\, e^{-i\,2\pi\,\theta(f)} \tag{17}$$

where i is the imaginary unit.

In case of a linear, time invariant system, the complex frequency response is the Fourier transform of the real valued impulse response, $h(t)$. Consequently, $h(t)$ is calculated by an inverse Fourier transformation of $H(f)$, see e.g. Karl [6].

NUMERICAL FORMULATION

The boundary integral equations for φ and φ_t are solved by the Boundary Element Method described in Brebbia and Walker [2]. Constant elements are used and each integral in the equations (3) and (5) is transformed into a sum of integrals over each boundary element. Non-singular integrals are calculated by a standard 4. order Gauss quadrature rule, and the singular integrals are calculated analytically.

The variation of the variables with time is found by a time stepping technique. Superscript k denotes the value of a variable at the time $t = k \cdot \Delta t$ or time step k. In the following all variables are supposed to be known at time step k, and the task is to compute the corresponding values at time step $k+1$.

General boundary conditions

The expansion of φ and η in Taylor series up to second order yields together with equation (6) and (7):

$$\varphi^{k+1} = \varphi^k - g\,\eta^k\,\Delta t - \frac{1}{2}\,g\left(\frac{\partial \varphi}{\partial n}\right)^k \Delta t^2 \qquad \text{on } S_F \qquad (18)$$

and

$$\eta^{k+1} = \eta^k + \left(\frac{\partial \varphi}{\partial n}\right)^k \Delta t + \frac{1}{2}\left(\frac{\partial \varphi_t}{\partial n}\right)^k \Delta t^2 \qquad \text{on } S_F \qquad (19)$$

The boundary condition for φ_t is

$$\varphi_t^{k+1} = -g\,\eta^{k+1} \qquad \text{on } S_F \qquad (20)$$

At the wavemaker the boundary conditions at timestep $k+1$ are

$$\left(\frac{\partial \varphi}{\partial n}\right)^{k+1} = -\dot{x}_w\left((k+1)\,\Delta t\right) \qquad \text{on } S_O \qquad (21)$$

and

$$\left(\frac{\partial \varphi_t}{\partial n}\right)^{k+1} = -\ddot{x}_w\left((k+1)\,\Delta t\right) \qquad \text{on } S_O \qquad (22)$$

Although the position of the wavemaker in principle can be varied arbitrary in time, only sinusoidal motion or motion corresponding to a sum of sines are applied in this paper. The amplitude of the wavemaker is calculated according to Biesels theory.

Active absorption, boundary conditions

In this case the horizontal velocity component on the boundary is found by equation (14). The impulse response of the filter is found by an inverse *discrete* Fourier transformation, which means that only N discrete values of the complex frequency response are used in the transformation, see Fig. 2.

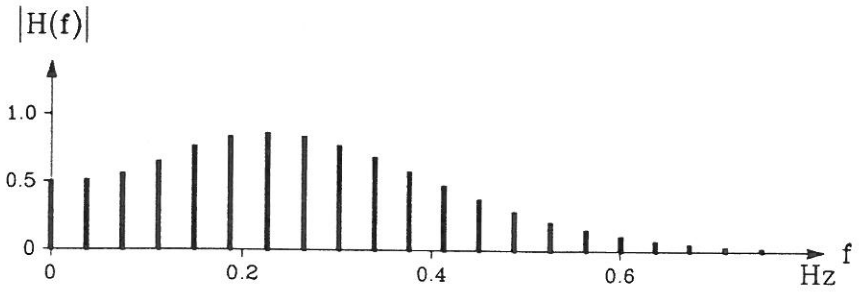

Figure 2. Magnitude gain, of the frequency response. $z = -2.5$ *m,* $h = 40$ *m,* $N = 41$, $\Delta t_{filter} = 0.65$ *secs.*

This gives an impulse response of *finite* duration, i.e. the impulse response or filter coefficients are found by

$$h^j = \sum_{r=-M}^{M} H_r \cdot e^{i\frac{2\pi r\, j}{N}} \quad \text{where } M = \frac{N-1}{2}\,,\ r = -M,\ \ldots\ ,+M \tag{23}$$

and H_r is the frequency response at the frequency $f = r \cdot \Delta f$.

The frequency increment, Δf, in the frequency response is found by

$$\Delta f = \frac{1}{N \cdot \Delta t_{filter}} \tag{24}$$

where Δt_{filter} is the time increment of the filter.

The price paid for handling only N frequencies in the transformation, is a minor (hopefully) inaccuracy in the performance of the filter for input frequencies, which do not coincide with one of the frequencies in the inverse discrete transformation.

If the length of the filter is increased, more frequencies are included, and in principle the overall accuracy of the filter is improved. In practice, however, there is a limit beyond which the accuracy of the filter starts to decrease due to other effects in the model.

Let us first notice a few characteristics of the behaviour of FIR-filters, see e.g. Karl [6].

- If $\theta(f) \equiv 0$ ($\sim$ the distance $\Delta x = 0$) and if a time delay of $(N-1)/2$ time steps are accepted, the filter is symmetrical about $j = 0$ or the middle of the filter. In principle the delaying effect of a symmetrical filter is shown in Figure 3. See also Figure 5.

- If all filter coefficients are shifted towards increasing j-values in the filter the result is a reduction of the delay caused by the filter. For example the filter in Figure 4, where the filter coefficient is shifted $(N-1)/2$ positions to the right, causes no delay. In practice, however, a total removal of the filter delay is not possible. The filter coefficients are periodic, $h^{j-N} = h^j$, and if $N > 1$, the result is the appearance of filter coefficients of considerable sizes at the 'left hand side' of the filter. See Figure 6. In most cases the performance of such a filter is poor.

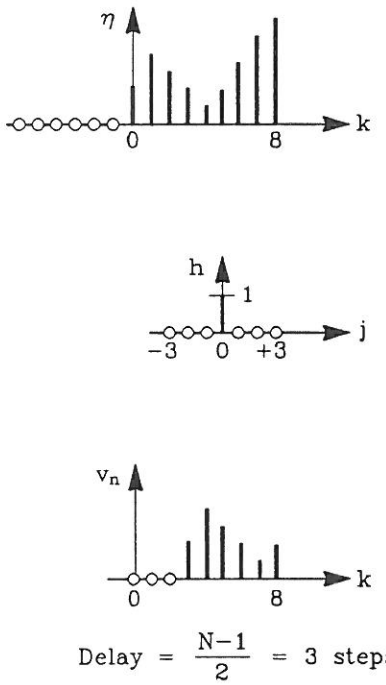

Fig. 3. A simple filter causing a delay of the output. The position of the filter corresponds to k=8.

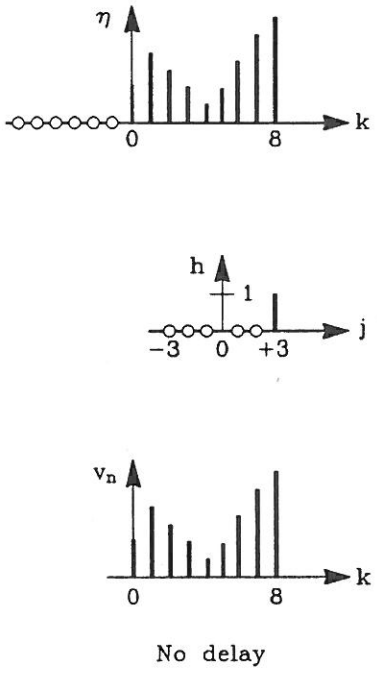

Fig. 4. A simple filter causing no delay of the output. The position of the filter corresponds to k=8.

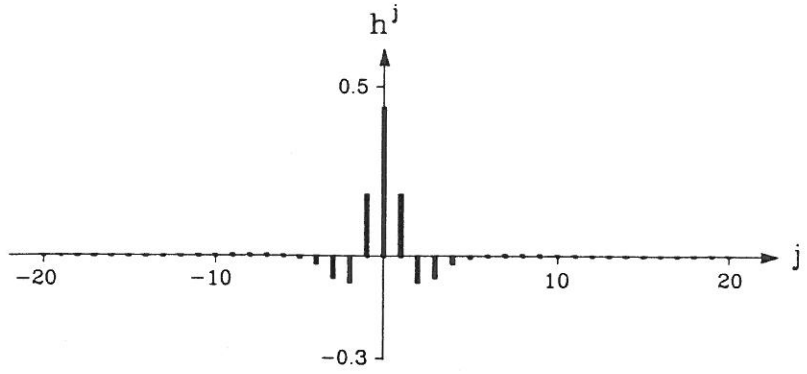

Figure 5. A filter causing a delay of $(N-1)/2$ steps. $\Delta x = 0$, $z = -2.5$ m, $h = 40$ m, $N = 41$, $\Delta t_{filter} = 0.65$ secs.

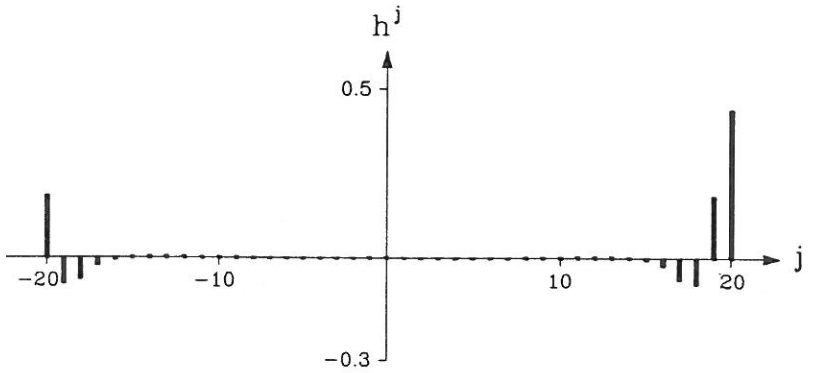

Figure 6. A filter causing no delay. $\Delta x = 0$, $z = -2.5$ m, $h = 40$ m, $N = 41$, $\Delta t_{filter} = 0.65$ secs.

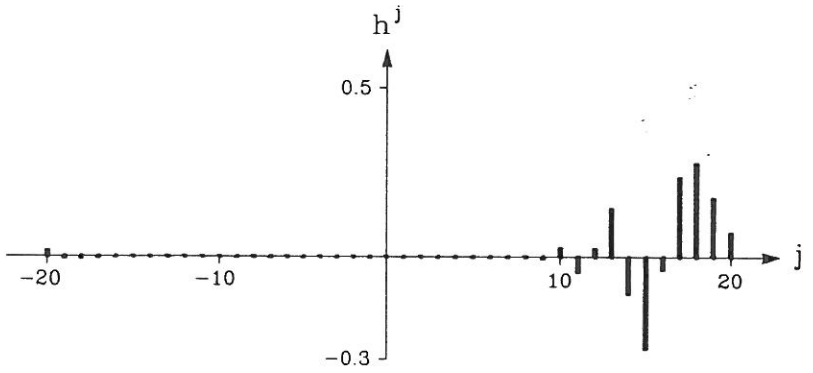

Figure 7. A filter causing no delay. $\Delta x = 7.5$ m, $z = -2.5$ m, $h = 40$ m, $N = 41$, $\Delta t_{filter} = 0.65$ secs.

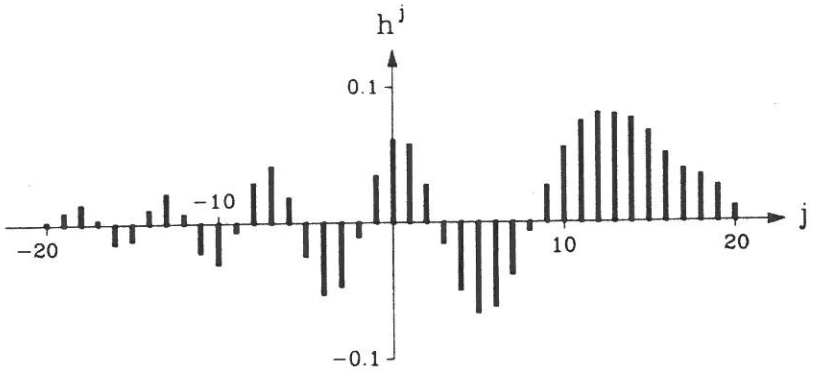

Figure 8. A filter causing no delay. $\Delta x = 57.5$ *m,* $z = -7.5$ *m,* $h = 40$ *m,* $N = 41$, $\Delta t_{filter} = 0.65$ *secs.*

To avoid the side effects of a total removal of the delay caused by the filter itself, the input is chosen to be the surface elevation registered at the distance Δx in front of the open boundary. In this case the filter must delay the output at frequency f corresponding to the time it takes for that waves to propagate the distance Δx. The effect of this on the filter is a 'shift' to the left of the filter coefficients, but it should be noted that this phase shift is frequency dependent, and it destroys the symmetri of the filter. A 'tail' is created to the left of the central part of the filter, see Figure 7 and 8.

In order to keep zero time delay in this situation, the filter must therefore produce the total phase shift at frequency f:

$$\theta(f) = 2\pi \left(\frac{\Delta x}{L} - \frac{(N-1)\,\Delta t}{2T} \right) \tag{25}$$

In the design of the filter the following rules of thumb can be set up:

- the width of the filter must be so large that the filter coefficients have decayed near the two ends of the filter.

- Δx must be so large that the needed 'shift' to the left of the filter coefficients can be established.

- Δx must be so small that the phase error, caused by the difference between the phase velocity of the waves in the numerical model and 1. order waves, is unimportant.

It is of course desirable to obtain more specific guidelines for the design of the filter, but in the present study the design was an trial and error-procedure based on the rules of thumb mentioned above.

The performance of each filter is assessed by comparing theoretical velocities (1. order theory) with velocities obtained by filtering of the corresponding theoretical surface elevations. The surface elevation is the sum of 4 sine waves with frequencies which are not coinciding with the frequencies of the discret frequency response.

NUMERICAL EXAMPLES

All simulations are made with a wave channel, 190 m long. Waves are generated by a piston type wavemaker at the left hand boundary, and the waves are absorbed at the open boundary, see Figure 1. The water depth is $h = 40$ m and the boundary is dicretized into 5 m long elements. The time increment is in all simulations $\Delta t = 0.13$ seconds. The shortest wavelength is approx. 55 m corresponding to T =6 secs, so the resolutions are at least 11 elements per wavelength and 46 time steps per wave period.

The reflection coefficent is defined as the ratio between reflected and incoming wave height at a given frequency, and in case of irregular waves an overall reflection coefficient is defined as the square root of the ratio between the reflected and the incoming wave energy.

Reflection coefficients are in all cases estimated by the method described in Goda and Suzuki [5]. In order to avoid spectral leakage in case of regular waves, the necessary FFT-analysis is made with 64 data corresponding to exactly one wave period. This is obtained by interpolation of the simulated time series.

In all simulations with active absorption, a filter is designed for each boundary element on the open boundary. Preliminary tests showed, however, that acceptable filters could not be designed, if the same surface elevation time series was used as input to all the filters. Instead Δx is optimized (trial and error!) for each filter. Note, however, that it is only necessary to demand $\Delta t_{filter} = p \cdot \Delta t$, where p is an integer. In this way the necessary resolution of the frequency response is achieved with fewer filter coefficients, but equation (14) must be changed a little in order to filter the correct surface elevations.

All simulations are started with the fluid at rest. The theoretical motion of the wavemaker is multiplied with a factor varying linearly from 0 to 1 during the first wave period in order to create a smooth start of the simulation. Tests showed, however, that a longer starting period has only insignificant influence on the results.

Active absorption, regular waves

The wave periods are varied from 6 to 16 seconds in order to get results, which can be compared with results from irregular waves with a spectrum covering the range 0.07-0.16 Hz. This range corresponds approx. to the range of a Jonswap spectrum with a peak period of 9 seconds (0.111 Hz). The results of the 'optimization' of the filters are: $N = 41$, $\Delta t_{filter} = 5\,\Delta t = 0.65$ second giving $\Delta f = 0.038$ Hz in $H(f)$ and the optimum distances are shown in Table 1.

z (m)	−2.5	−7.5	−12.5	−17.5	−22.5	−27.5	−32.5	−37.5
Δx (m)	7.5	57.5	67.5	72.5	82.5	87.5	92.5	92.5

Table 1. Horizontal distances between open boundary and position of wave gauge. z is the level of the boundary element mode.

It is seen that Δx is increasing with the distance below the surface, but note that $\Delta x/L_{max} < 0.32$, where $L_{max} = 284$ m corresponds to T =16 seconds. The large difference between the values of Δx corresponding to $z = -2.5$ m is a bit surprising. The performance of the filters is, however, changing rather slowly with Δx, and the result could have been different, if the filters during the design phase had been tested with other wave periods than T =7, 9, 11, and 13 seconds.

From the Figure 9 is seen that the active absorption is giving reflection coefficients smaller than 3% for frequencies ranging from approx. 0.06 - 0.13 Hz. At the higher frequencies the reflection coefficient is increasing, most likely due to the decreasing resolution in time and space. The reason why the reflection coefficient is increasing at the lower frequencies needs further research.

The reflection coefficients created by active absorption can be compared with the reflection coefficients obtained with two types of Sommerfelds radiation condition, either variable phase velocity, $c = c(f)$, or constant phase velocity, c = constant. See Figure 9. The active absorption is giving results very close to the best obtainable (Sommerfeld, $c = c(f)$), and the reflection coefficients in a model with active absorption are for all frequencies smaller than the reflection coefficients calculated in a model, where Sommerfelds radiation condition is used with a constant phase velocity corresponding to $f = 0.111$ Hz.

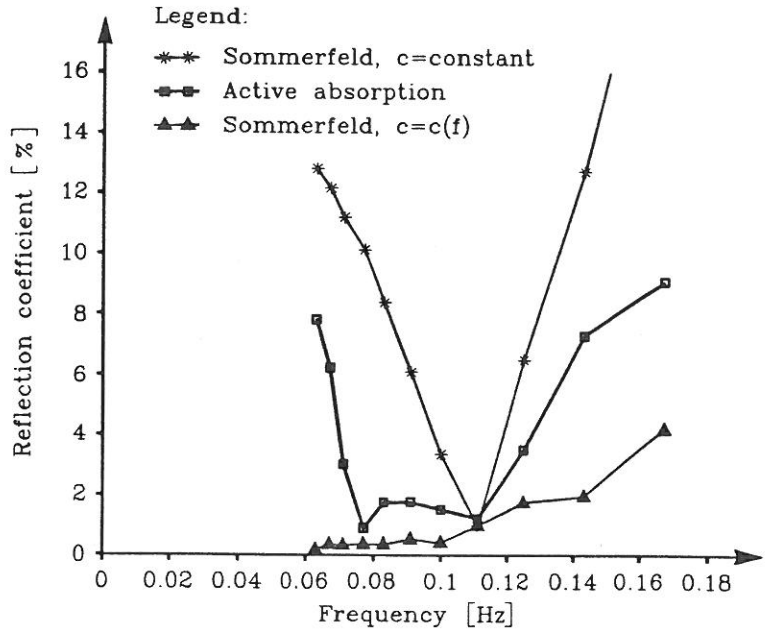

Figure 9. Reflection coefficients. Regular waves, $h = 40$ m. The constant phase velocity corresponds to $f = 0.111$ Hz.

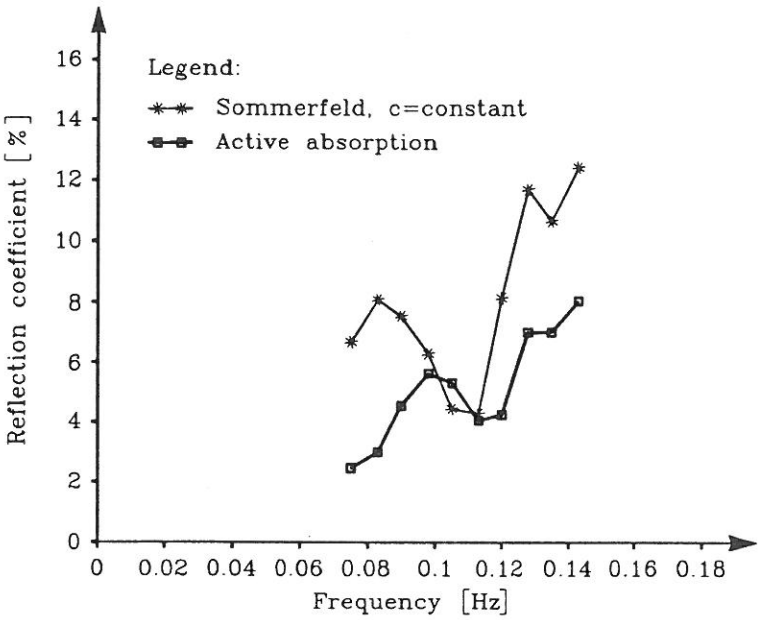

Figure 10. Reflection coefficients. Irregular waves, $h = 40$ m. The constant phase velocity corresponds to $f = 0.111$ Hz.

Irregular waves

Each simulation is 1400 time steps long. The necessary FFT-analysis is based on time series containing 1024 data, which are cosine-tapered to minimize spectral leakage. In order to improve the accuracy further, the reflection coefficients are estimated as the mean values from 10 simulations. The wavemaker variance spectrum is in all cases corresponding to a surface elevation composed of 10 sine waves, all having the same wave height. The phases are, however, selected randomly. The frequency range is from 0.07-0.15 Hz. In order to compare the results from the simulation with active absorption and the Sommerfeld condition (c = constant), the same 10 time series of the motion of the wavemaker are used in both series of simulations.

The results are shown in Figure 10. In general both methods of absorption create somewhat larger reflection coefficients than seen in the simulations with regular waves. This increase is not believed to be caused by random errors caused by the analysis of a finite time series, because the increase is nearly the same at all frequencies, and the wave heights of the incoming waves are estimated with an error less than 10%.
Except at one single frequency the active absorption is giving the smallest reflection coefficients, and near the ends of the frequency interval the active absorption is clearly the best approach.
We find $R_{overall} = 5.1\%$ if active absorption is used, and $R_{overall} = 8.0\%$ if Sommerfelds radiation condition (c = constant) is used. This difference between the two metods is expected to decrease if the elevation spectrum is a Jonswap spectrum.

Similar simulations made with a water depth of 20 m show the same trends. As expected the only significant change in the results is that the Sommerfeld condition (c = constant) created smaller reflection coefficients than in case of $h = 40$ m.

CONCLUSION

With active absorption based on FIR-filters, it is possible to reduce the reflection of irregular waves at the open boundaries in BEM-models to an acceptable degree. On medium or large water depths the computational area in which the waves are absorbed can be reduced to approx. 1/3 in comparison with e.g. sponge layers, and the frequency range with acceptable reflection coefficients is approx. 2-3 times the range obtained with e.g. Sommerfelds radiation condition. Active absorption is rather simple to implement in the computer code, and the direct computational costs are small. At present, however, the insuffient guidelines in the design of the numerical filter and the assumption of linear waves are limiting factors in the applicability of the approach.

REFERENCES

1. Baker, G. R., Meiron, D. I. and Orszag, S. A. 'Generalized vortex methods for free surface flow problems', *Journal of Fluid Mechanics,* Vol. 123, pp. 477-501, 1982.

2. Brebbia, C.A. and Walker, S. *Boundary Element Techniques in Engineering.* Newnes-Butterworth, England, 1980.

3. Brorsen, M. and Larsen, J. 'Source Generation of nonlinear Gravity Waves with the Boundary Integral Element Method', *Coastal Engineering,* vol. 11, pp. 93-113, Elsevier, Amsterdam, 1987.

4. Dold, J.W. and Peregrine, D. H. 'Steep unsteady water waves: an efficient computational scheme', *Proceedings, 19th International Conference on Coastal Engineering,* Vol. 1, pp. 995-967, Houston, USA, 1984.

5. Goda, Y. and Suzuki, Y. 'Estimation of incident and reflected waves in random wave experiments', *Proceedings, 15th International Conference on Coastal Engineering,* Vol. 1, pp. 828-845, Honolulu, Hawaii, 1976.

6. Karl, J.,H. *An Introduction to Digital Signal Processing,* Academic Press, San Diego, 1989.

7. Larsen, J. and Dancy, H. 'Open boundaries in short wave simulations - A new approach', *Coastal Engineering,* vol. 7, pp. 285-297, Elsevier, Amsterdam, 1983.

8. Lennon, G.P., Liu, P.L.-F. and Liggett, J.A. 'Boundary Integral Solutions of Water Wave Problems.' *Journal of the Hydraulics Division, ASCE,* Vol. 108 (HY 8), pp.921-932.

9. Longuet-Higgins, M. S. and Cokelet, E. D. 'The deformation of steep surface waves on water. A numerical method of computation.', *Proceedings, Royal Society of London, Series A,* Vol. 350, pp. 1-25, 1976.

10. Svendsen, I.A. and Jonsson, I.G. *Hydrodynamics of Coastal Regions,* Den private ingeniørfond, Technical University of Denmark, Lyngby, 1980.